PAPER

Check for updates

Electrical properties of Sb₂O₃-modified BiScO₃– PbTiO₃-based piezoelectric ceramics

Long Xue,[ab] Qian Wei,[c] Zujian Wang,[b] Xiaoming Yang,[b] Xifa Long [iD] [b] and Chao He [iD] *[b]

Compared with pure Pb-based perovskite ferroelectric materials, BiMeO₃–PbTiO₃ (Me = Sc³⁺, In³⁺, and Yb³⁺) systems have remarkable advantages in their Curie temperatures. As a member of this group, the BiScO₃–PbTiO₃ (BS–PT) solid solution has drawn considerable attention from scientists for its high Curie temperature and excellent piezoelectric coefficient. However, BS–PT ceramics still have some shortcomings, such as high dielectric loss and low mechanical quality factor, which make them unsuitable for high-temperature applications. Herein, we report the effect of the addition of complex ions on the electrical properties of BS–PT ceramics. Sb₂O₃-doped 0.36BiScO₃−0.64PbTi₀.₉₇Fe₀.₀₃O₃ + 1 mol% MnO₂ (BS–PTFMn + x% Sb₂O₃) ceramics were fabricated and their electrical properties were studied. BS–PTFMn + 0.75% Sb₂O₃ had an optimal piezoelectric coefficient, exhibiting $d_{33}^* = 442$ pm V⁻¹. which indicates that Sb₂O₃ doping can improve the piezoelectric properties of the BS–PT ceramics, exhibiting a "soft" effect of Sb₂O₃ doping. In addition, the thermal depolarization temperature (T_d) of BS–PTFMn + 0.75% Sb₂O₃ ceramics remained above 300 °C, such as 325 °C for BS–PTFMn + 0.75% Sb₂O₃. It was concluded that the piezoelectric properties of BS–PT ceramics were enhanced by the addition of Sb₂O₃.

1. Introduction

High-temperature piezoelectric materials have received unprecedented attention due to the urgent demand for high-temperature piezoelectric sensors and actuators in aerospace, automobile, oil and gas exploration fields.[1–3] The commercial lead–zirconium–titanium (PZT) piezoelectric ceramics have been studied for decades and are widely used in piezoelectric sensors and transducers due to their outstanding piezoelectric properties, such as $d_{33} = 285$ pC N⁻¹ for PZT-4, $d_{33} = 375$ pC N⁻¹ for PZT-5A.[4] Nevertheless, their curie temperatures, T_C, are below 380 °C.[5,6] It is generally believed that the safe usage temperature range cannot exceed half of the Curie temperature in bulk PZT-based piezoelectric materials because of the depolarization caused by the thermal activation. Therefore, the traditional PZT-based piezoelectric ceramics cannot be used in the environments above 200 °C.[4,5] This is far from enough for today's industrial demands. Therefore, the development of new high-temperature-stable piezoelectric materials is an extremely urgent need.

In 2001, Eitel Richard first reported Bi(Me)O₃–PbTiO₃ (Me = Sc, In, Yb, Mg/Ti, Fe and Ga) systems, which have a perovskite structure and high Curie temperature.[7–12] Among them, BiScO₃– PbTiO₃ (BS–PT) ceramics have drawn considerable attention because of their large piezoelectric coefficient ($d_{33} = 460$ pC N⁻¹) and high Curie temperature ($T_C = 450$ °C) near the morphotropic phase boundary (MPB), and have a good application prospect at high temperatures.[13,14] However, the thermal degradation of BS–PT ceramics occurs at 250 °C, which limits their applications at high temperatures.[15,16] Moreover, BS–PT ceramics have a high dielectric loss, resulting in high energy consumption and heat dissipation in the use of high-power electronic devices.[17]

Previously, numerous studies were involved in controlling the reduction of dielectric loss, improving the electrical properties and thermal stability by the addition of a third element,[18–20] such as Pb(Mg₁/₃Nb₂/₃)O₃ (PMN), BaTiO₃ (BT), and Pb(Mn₁/₃Sb₂/₃)O₃ (PMS). It is reported that the defects and oxygen vacancies generated by the multi-valence elements, such as Mn and Fe, can diffuse to the domain boundaries and reduce the total energy of the ceramics, leading to the pinning behavior of the motion of 180° domain and effective reduction of the dielectric loss.[17,21] Chen *et al.* reported that 0.36BiScO₃– 0.64Pb(Ti₀.₉₇Fe₀.₀₃)O₃ + 1 mol% MnO₂ ceramics exhibited a high Curie temperature ($T_C = 492$ °C) and low dielectric loss (tan δ = 0.006).[21] Unfortunately, its d_{33} significantly deteriorated ($d_{33} = 238$ pC N⁻¹) and the dielectric constant significantly

[a]*College of Chemistry and Materials Science, Fujian Normal University, Fuzhou, 350117, China*

[b]*Key Laboratory of Optoelectronic Materials Chemistry and Physics, Fujian Institute of Research on the Structure of Matter, Chinese Academy of Sciences, Fuzhou, 350002, China. E-mail: hehcao@fjirsm.ac.cn*

[c]*Institute of Acoustics, Chinese Academy of Sciences, Beijing, 100190, China*

decreased ($\varepsilon_r = 815$). Mixed Mn and Sb elements are usually used to modify commercial PZT-based piezoelectric ceramics because the mixed Mn and Sb can synchronously enhance k_p, Q_m, ε_r, and d_{33}.[22–24] Therefore, in this study, Sb_2O_3 was added to $0.36BiScO_3$–$0.64Pb(Ti_{0.97}Fe_{0.03})O_3$ + 1 mol% MnO_2 ceramics. The effects of Sb_2O_3 content doping on the phase structure, dielectric, piezoelectric, ferroelectric and electromechanical coupling properties of $0.36BiScO_3$–$0.64Pb(Ti_{0.97}Fe_{0.03})O_3$ + 1 mol% MnO_2 ceramics were investigated.

2. Experimental procedure

2.1 Sample preparation

In this study, $0.36BiScO_3$–$0.64Pb(Ti_{0.97}Fe_{0.03})O_3$ + 1 mol% MnO_2 + x mol% Sb_2O_3 (x = 0, 0.25, 0.5, 0.75, 1, and 1.5) (BS–PTFMn + x% Sb_2O_3) were prepared by a conventional solid-state method. The oxide powders, Bi_2O_3 (99.5%), Sc_2O_3 (99.99%), PbO (99.9%), TiO_2 (99.5%), Sb_2O_3 (99.5%), Fe_2O_3 (99.5%) and MnO_2 (99.5%), were accurately weighed and mixed according to the desired stoichiometric compositions. In addition, 3 wt% excess Bi_2O_3 was added to compensate for the volatilization of bismuth at high temperatures. The weighed powder was put into an agate grinding tank with an agate ball and anhydrous ethanol as the ball-mill medium for the ball milling. The ball milling was used with a planetary ball mill for 24 hours. After ball-milling, the mixed powder was dried, pressed into blocks and placed in a crucible, and calcined at 750 °C for 4 h. The calcination of blocks can reduce the distance of the powders, which is conducive to matter diffusion, the uniformity of a reaction and the reduction in the calcination temperature and time. Then, small amounts of MnO_2 and Sb_2O_3 were added to the calcined mixture and ground in alcohol for 24 hours. After drying, the calcined powders were granulated with 5% polyvinyl alcohol binder (PVA) and then pressed into pellets of 10 mm in diameter and 1 mm in thickness under 200 MPa. The green pellets were heated at 550 °C for 4 h to remove PVA. Furthermore, the green pellets were placed in an Al_2O_3 crucible and sintered at 1000–1100 °C for 3 h, while embedded in the calcined powders for preventing the evaporation of Bi and Pb.

2.2 Characterization methods

The crystalline phase of sintered samples was analyzed using an X-ray diffractometer (Miniflex 600, Rigaku, Japan) with Cu-Kα_1, Kα_2 mixing radiation, operating at 40 kV and 40 mA, in the 2θ range of 10–60° with a step size of 0.05° and 0.5 s per step. The fractured surface morphologies of the obtained ceramic samples were characterized by scanning electron microscopy (SEM, SU8010, Hitachi, Japan). The sintered samples were polished to the thickness of 0.5 mm, and then coated with a silver paste for electrical characterization. The samples were placed in a silicon oil at 120 °C and poled for 20 min under a DC electric field of 40 kV cm^{-1}. The electrical properties of poled samples were tested after placement for 24 h. The piezoelectric coefficients d_{33} were measured using a quasi-static d_{33} meter (Institute of Acoustics, Chinese Academy of Sciences, model ZJ-4AN). The planar electromechanical coupling factor (k_p) and the mechanical quality factor (Q_m) were calculated according to the resonance and anti-resonance methods using an impedance analyzer (E4990A, Agilent Technologies, USA). The dielectric constant (ε_r) and dielectric loss (tan δ) as functions of temperature were also measured using the impedance analyzer. The polarization–electric field (P–E) hysteresis loops, current–electric field (I–E) loops and strain–electric field (S–E) curves were obtained using an aix-ACCT TF2000 analyzer with a frequency of 1 Hz. The resistivity of ceramics was measured using an electrometer/high resistance meter (Keithley 6517B, USA).

3. Results and discussion

3.1 Structure and phase analysis

Fig. 1(a) shows the XRD patterns of sintered ceramic samples with different Sb_2O_3 contents. All the samples presented a pure perovskite structure without any clear trace of impurity phases, indicating stable perovskite solid solutions. Since the radii of Fe^{3+} ion (0.645 Å for CN = 6) and Mn^{3+} ion (0.645 Å for CN = 6) are similar to Ti^{4+} radius (0.605 Å for CN = 6), Fe^{3+} and Mn^{3+} were likely to replace Ti^{4+} in BO_6 octahedral perovskite structures.[25] In addition, though Sb is a multivalent element, more
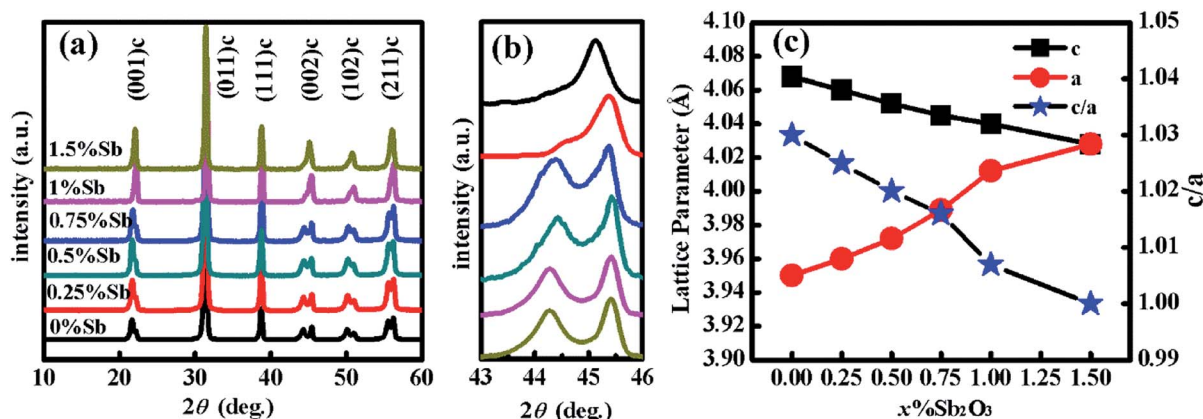

Fig. 1 (a) XRD patterns of BS–PTFMn + x% Sb_2O_3 ceramics. (b) The enlarged view of XRD patterns at $2\theta = 43-46$. (c) Lattice parameters as function of Sb_2O_3 content.
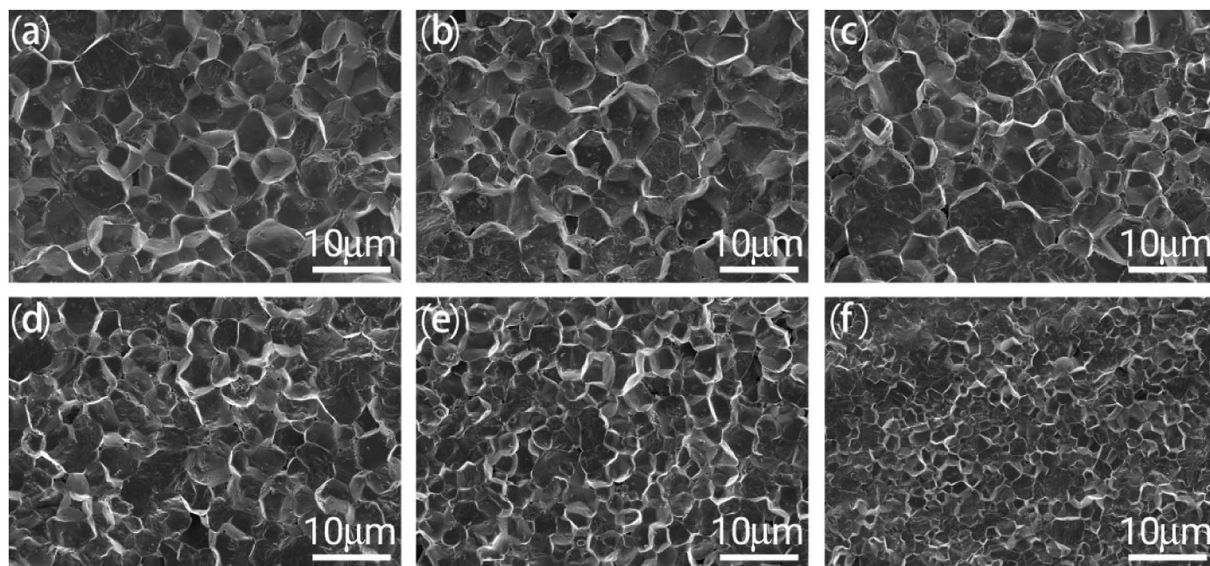
Fig. 2 SEM micrographs of fracture surface of BS–PTFMn + x% Sb_2O_3 ceramics: (a) 0% Sb_2O_3, (b) 0.25% Sb_2O_3, (c) 0.5% Sb_2O_3, (d) 0.75% Sb_2O_3, (e) 1% Sb_2O_3, (f) 1.5% Sb_2O_3.

Sb^{5+} can be formed in the sintering process. It is expected that Sb^{5+} will most likely enter into the B-site to substitute Ti^{4+} because the radius of Sb^{5+} ion (0.60 Å for CN = 6) is close to that of Ti^{4+} ion (0.605 Å for CN = 6). Moreover, oxygen vacancies can be formed in Fe^{3+} and Mn^{3+} doped BS–PT ceramics due to the substitution of Ti^{4+} with low ionic valence (Fe^{3+} as an example: $Fe_2O_3 + 2TiO_2 \rightarrow 2Fe'_{Ti} + V_O^{\cdot\cdot} + 3O_O$).[21] Therefore, the BS–PT ceramics can maintain charge neutrality after Sb_2O_3 doping. It also can be seen that the ceramic samples gradually transformed from a tetragonal phase to a rhombohedral phase as Sb_2O_3 doping increased (Fig. 1(a)). In order to clearly observe the view of $(002)_c$ diffraction peaks in the range of $2\theta = 43–46°$, it was enlarged as shown in Fig. 1(b). It is intuitively revealed that there was a phase transition. In addition, the lattice parameters calculated using Jade 5.0 based on the XRD results are shown in Fig. 1(c). It can be seen that the c/a value continuously decreases from 1.03 to 1 with the increase in the Sb_2O_3 content, also clearly confirming the phase transition. A similar change in structure was found in Sb-doped PMN–PT ceramics.[26] The diffraction index (hkl) labeled in Fig. 1 refers to the cubic perovskite structure.

Fig. 2 shows the SEM images of the fractured surface of BS–PTFMn + x% Sb_2O_3 ceramics with different Sb_2O_3 contents. These images clearly show the grain and grain boundary of ceramic samples without any holes, indicating that the samples were well-sintered and have high densities. It can be easily seen that the average grain size (d) of an undoped sample is about 10 μm. However, the average grain size rapidly decreased from 10 μm to 2 μm with the increase in Sb_2O_3 incorporation. The detailed grain size is listed in Table 1. Clearly, grain growth can be controlled by the addition of Sb_2O_3. The Sb ions could not be completely dissolved into the solid solution as the doping amount of Sb_2O_3 increased to 1.5% in this study. The extra Sb_2O_3 diffused into the grain boundary, which prevented the movement of the grain boundary during the sintering process and hindered the growth of grain, leading to the reduction of grain size of Sb-doped samples.[27] Therefore, the average grain size decreased rapidly at this composition. In addition, the Archimedes method was used to calculate the actual density (ρ_1) of ceramic samples, while the theoretical density (ρ_2) was calculated based on the XRD data. The calculated results showed that the relative density (ρ_r) of ceramic samples was 96.5–98.6%, indicating a high density of ceramic samples. The results are listed in Table 1. The density of the ceramic samples reached the maximum at $x = 0.75$ with a grain size of 5.0 μm. The interlayer and porosity were created when extra Sb_2O_3 diffused into the grain boundary, such as $x = 1.50$.

Table 1 Density and average grain size of BS–PTFMn + x% Sb_2O_3 ceramics (d: average grain size; ρ_1: actual density; ρ_2: theoretical density; ρ_r: relative density)

Composition	d (μm)	ρ_1 (g cm^{-3})	ρ_2 (g cm^{-3})	ρ_r (%)
$x = 0.00$	10	7.23	7.45	97.1
$x = 0.25$	9	7.25	7.44	97.4
$x = 0.50$	8	7.28	7.41	98.2
$x = 0.75$	5	7.32	7.42	98.6
$x = 1.00$	3	7.27	7.43	97.8
$x = 1.50$	2	7.22	7.48	96.5

3.2 Dielectric properties

Fig. 3 shows the temperature dependence of dielectric constant (ε_r) and dielectric loss (tan δ) of BS–PTFMn + x% Sb_2O_3 ceramics. The values of dielectric constant (ε_r) at room temperature increased first and then decreased with the increase in Sb_2O_3, as shown in Table 2. The maximum of ε_r appeared at BS–PTFMn + 0.75% Sb_2O_3 ceramics. The increase in
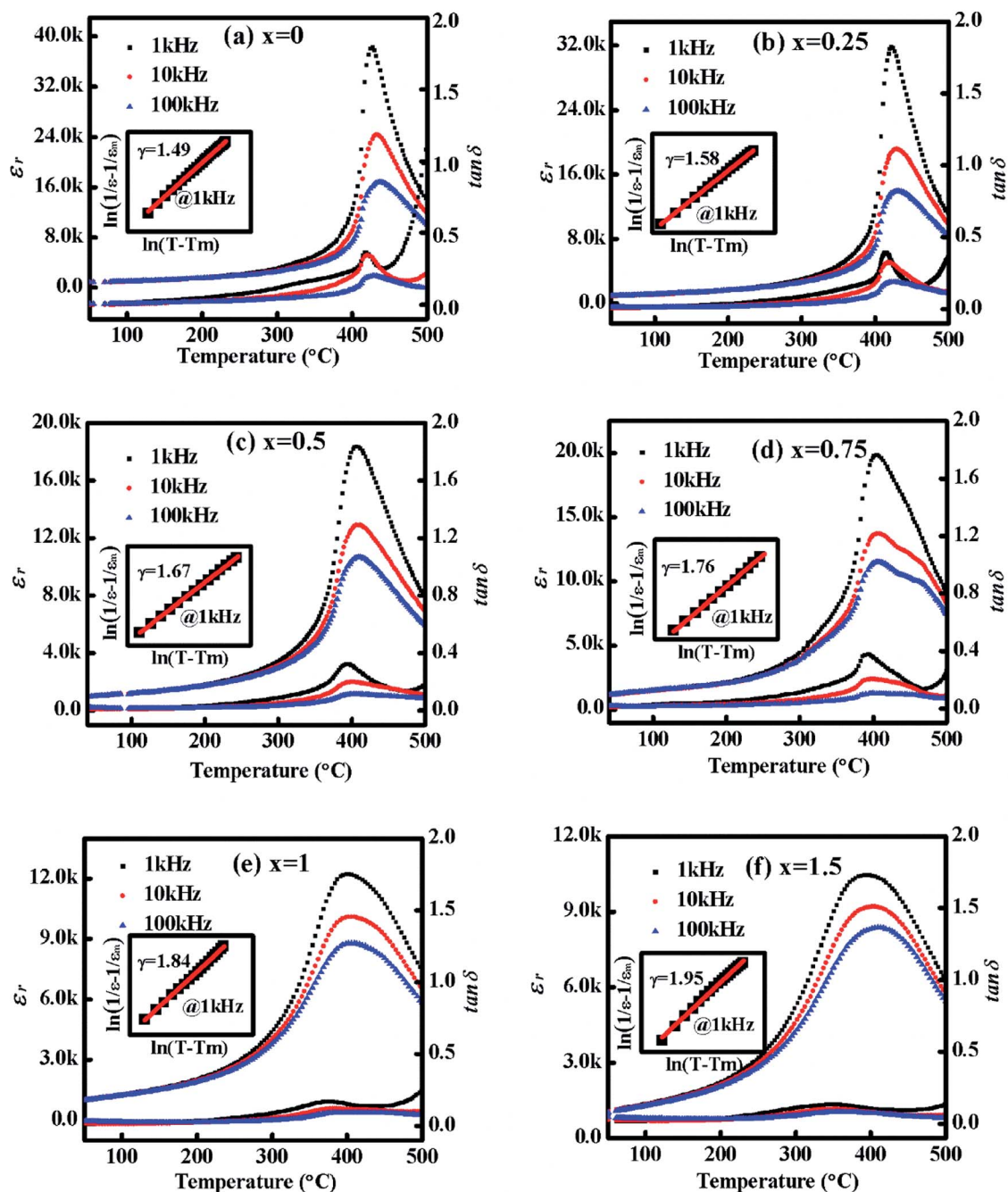
Fig. 3 Temperature dependence of dielectric properties (ε_r, tan δ) of BS–PTFMn + $x\%$ Sb$_2$O$_3$ ceramics: (a) 0% Sb$_2$O$_3$ (b) 0.25% Sb$_2$O$_3$, (c) 0.5% Sb$_2$O$_3$, (d) 0.75% Sb$_2$O$_3$, (e) 1% Sb$_2$O$_3$, (f) 1.5% Sb$_2$O$_3$. The insets show the fitting result using semi-empirical Curie–Weiss law.

Table 2 Electrical properties of BS–PTFMn + $x\%$ Sb$_2$O$_3$ ceramics

Composition	T_c (°C)	ε_r	tan δ	P_r (μC cm^{-2})	E_c (kV cm^{-1})	d_{33} (pC N^{-1})	k_p	Q_m	T_d (°C)
$x = 0.00$	425	920	0.008	17	28	230	0.39	180	380
$x = 0.25$	422	960	0.009	20	26	260	0.42	141	365
$x = 0.50$	407	1000	0.009	21	23	270	0.43	125	350
$x = 0.75$	404	1230	0.014	24	22	305	0.45	93	325
$x = 1.00$	400	1060	0.015	24	24	280	0.40	86	310
$x = 1.50$	394	1050	0.018	29	25	240	0.36	72	300

the dielectric constant is related to the decrease in the grain size (see Table 1). G. Arlt *et al.* reported that the width of the domain is proportional to the square root of the grain size in ferroelectric ceramics.[28] It is reasonable to conclude that the domain density increases when the grain size decreases. In addition, the dielectric constant is mainly affected by the extrinsic contribution originated from the movement of the domain wall.[29,30] Therefore, the extrinsic contribution to dielectric response can be enhanced if the density of domain walls increases, resulting in the enhancement of the dielectric constant. Therefore, the dielectric constant increased first, as shown in Table 2. When the Sb_2O_3 doping content further increased, the dielectric constant decreased because the extra Sb_2O_3 doping diffused into the grain boundaries, which hindered the movement of the electric domain.[26,30] In polycrystalline ferroelectric ceramics, the relationship between dielectric properties and grain size is very common and correspondingly observed.[31,32]

T_m, defined as the temperature of the maximum of ε_r, is considered as the Curie temperature T_C. It is clearly seen that Curie temperature is sensitive to Sb doping (listed in Table 2), and decreased linearly from 425 °C to 394 °C with the increase in Sb doping. Chen *et al.* reported that $0.36BiScO_3$–$0.64Pb(Ti_{0.97}Fe_{0.03})O_3 + 1$ mol% MnO_2 ceramics exhibit a high Curie temperature of 492 °C.[21] There are two main reasons for

the gap of Curie temperature between our results and those of previous reported. The first reason is that the deviation of components was induced by Pb and Bi volatilizing during the synthesis process. The second reason is the doping of complex ions. It is well known that Fe and Mn elements have multiple valence states. The Curie temperature can be affected by the change in the valence of Fe and Mn ions. The effects of complex ions on the variation of Curie temperature require further studies.

The peak of maximum ε_r became wider and wider as Sb_2O_3 increased, exhibiting a diffuse phase transition. In addition, with the increase in the Sb_2O_3 doping, T_m shifted to a high temperature as frequencies increased, showing frequency dispersion. It is indicated that BS–PTFMn + x% Sb_2O_3 ceramics exhibit a typical relaxor behavior as Sb_2O_3 is doped. The relaxor behavior of Sb-doped BS–PTFMn ceramics at a phase transition can be described by the modified Curie–Weiss law:[33]

$$\ln(1/\varepsilon - 1/\varepsilon_m) + \ln C = \gamma \ln(T - T_m) \quad (1)$$

where ε_m is the value of ε_r at T_m, C is the Curie constant, and γ is the degree of phase transition diffuses. When γ is equal to 1, it is usually considered a normal ferroelectric, which satisfies Curie–Weiss law. For $\gamma = 2$, the phase transition is a canonical relaxor ferroelectric with a completely diffused phase transition.
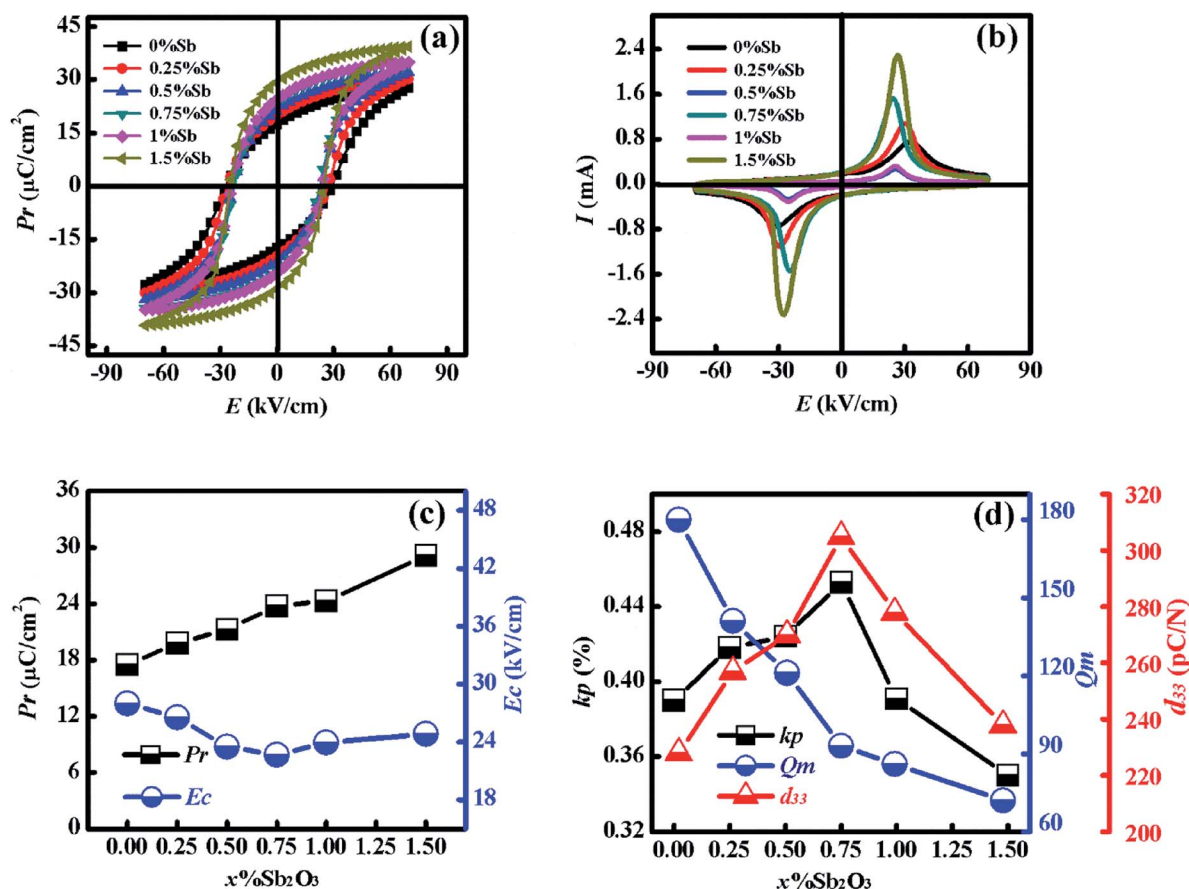

Fig. 4 (a) Polarization–electric field (P–E) hysteresis and (b) current–electric field (I–E) loops, (c) P_r and E_c, (d) d_{33}, k_p and Q_m as a function of Sb_2O_3 content of BS–PTFMn + x% Sb_2O_3 ceramics.

Therefore, a larger value of γ represents a larger degree of the diffused phase transition. The insets in Fig. 3 shows the fitting curves of $\ln(1/\varepsilon - 1/\varepsilon_m)$ vs. $\ln(T - T_m)$ at 1 kHz and the value of γ, showing that the value of γ for all the ceramic samples was between 1 and 2, indicating typical relaxor ferroelectrics. It can be clearly seen that the value of γ gradually increased from 1.49 to 1.95 as Sb_2O_3 increased. The relaxor behavior was related to the heterogeneity of the solid solution. Small amounts of Sb occupy the B-site in the perovskite structure, leading to a disordered distribution of ions at the B-site.[34] Therefore, the degree of heterogeneity increased with the Sb_2O_3 doping, which resulted in an increase in the degree of relaxation. Similar phenomena have been observed in other BS–PT based systems.[20,35]

3.3 Ferroelectric and piezoelectric properties

Fig. 4(a) shows the polarization–electric field (P–E) hysteresis loops of BS–PTFMn + x% Sb_2O_3 ceramics. The P–E hysteresis loops were measured under an electric field of ± 70 kV cm^{-1} at room temperature with a frequency of 1 Hz. According to the P–E hysteresis loops, the variation of the values of remnant polarization (P_r) and coercive field (E_c) was obtained, as shown in Fig. 4(c). The value of P_r gradually increased as the Sb content increased. However, the value of E_c decreased first and reached a minimum value (22 kV cm^{-1}) at $x = 0.75$. When the Sb_2O_3 doping content was higher than 0.75, the value of E_c increased slightly. The first decrease in E_c was mainly due to the "soft" doping of Sb_2O_3, while the second increase was mainly due to the excessive Sb_2O_3 at the grain boundary.[36] Fig. 4(b) shows the I–E loops of all the samples at room temperature. The clear positive and negative current peaks, which correspond to the switching of polarization reveals the well-shaped saturated ferroelectric hysteresis loops, confirming the high quality of P–E hysteresis loops.

The tendency of piezoelectric coefficient (d_{33}), planar electromechanical coupling factor (k_p), and mechanical quality factor (Q_m) as a function of the Sb_2O_3 doping content are shown in Fig. 4(d). The variation of d_{33} shows an opposite trend compared to that of E_c, showing optimal properties at $x = 0.75$ (305 pC N^{-1}), which indicates that Sb_2O_3 doping can improve the piezoelectric properties of BS–PT-based ceramics. Similarly, the value of k_p showed the same tendency, exhibiting the maximum at $x = 0.75$%. However, the value of Q_m monotonously declined from 180 to 70 as Sb_2O_3 increased, showing typical characteristics of a "soft" modifier. The detailed ferroelectric and piezoelectric properties are listed in Table 2. The optimal piezoelectric properties appeared for BS–PTFMn + 0.75% Sb_2O_3 ceramics, exhibiting $\varepsilon_r = 1230$, $\tan \delta = 0.014$, $E_c = 22$ kV cm^{-1}, $k_p = 0.45$ and $d_{33} = 305$ pC N^{-1}. It is well known that Sb_2O_3 is a type of soft doping in which Sb^{5+} will replace Ti^{4+} ions, reducing the formation of lead vacancy, which leads to the domain movement becoming easier.[37] Compared with undoped samples, the enhancement of d_{33} can be explained by a qualitative formula: $d_{33} \sim Q_{33}\varepsilon_r\varepsilon_0 P_r$ for the piezoelectric materials,[38] where ε_0 is the dielectric permittivity of free space, and Q_{33} is the electrostriction coefficient. The d_{33}, ε_r, P_r are interrelated,

showing high ε_r and high P_r for high piezoelectricity. All values of ε_r, P_r and d_{33} showed the same change as Sb_2O_3 increased to 0.75%. Therefore, the variation of d_{33} conforms to the formula. There are two reasons for an appreciable reduction of d_{33} upon further increase of Sb_2O_3. The one is that extra Sb_2O_3 doping diffused into the grain boundaries, which hindered the movement of the electric domain, reducing the extrinsic contribution to piezoelectricity. The other is due to the phase transition from the tetragonal phase to the rhombohedral phase, as shown in Fig. 1. The complex perovskite ferroelectrics exhibit optimal piezoelectricity near the MPB region. It has been reported that BS–PT based ceramics exhibit optimal piezoelectricity in the MPB region close to the tetragonal phase.[14] Therefore, the d_{33} decreased when the structure changed to the rhombohedral phase.

Fig. 5 shows the unipolar strain vs. electric field (S–E) curves of BS–PTFMn + x% Sb_2O_3 ceramics measured under an electric field of 70 kV cm^{-1}. The unipolar strain first increased with the increase in the Sb_2O_3 content, the maximum strain of 0.31% was obtained at BS–PTFMn + 0.75% Sb_2O_3 ceramics, and then decreased. For the undoped samples, a relatively small strain
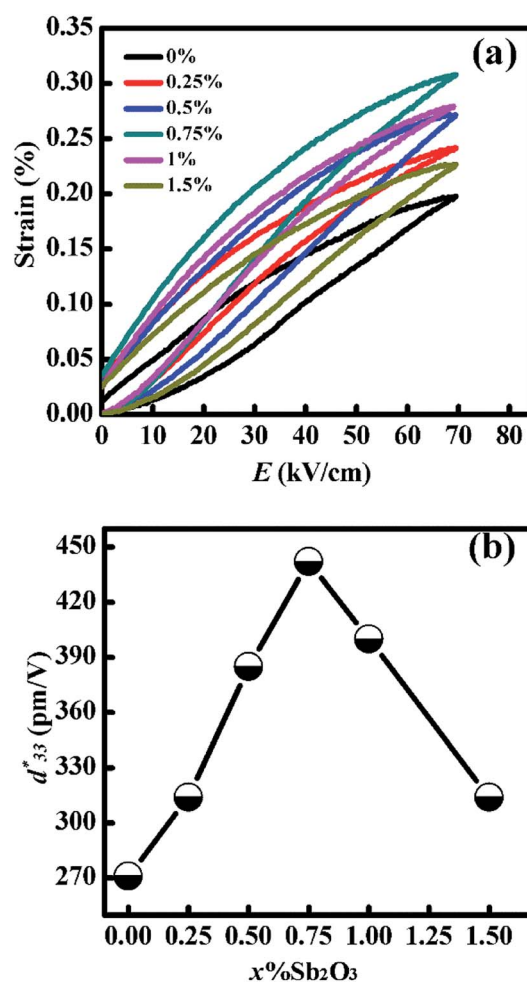

Fig. 5 (a) Unipolar strain vs. electric field (S–E) curves of BS–PTFMn + x% Sb_2O_3 ceramics at room temperature, (b) d^*_{33} as a function of Sb_2O_3 content.
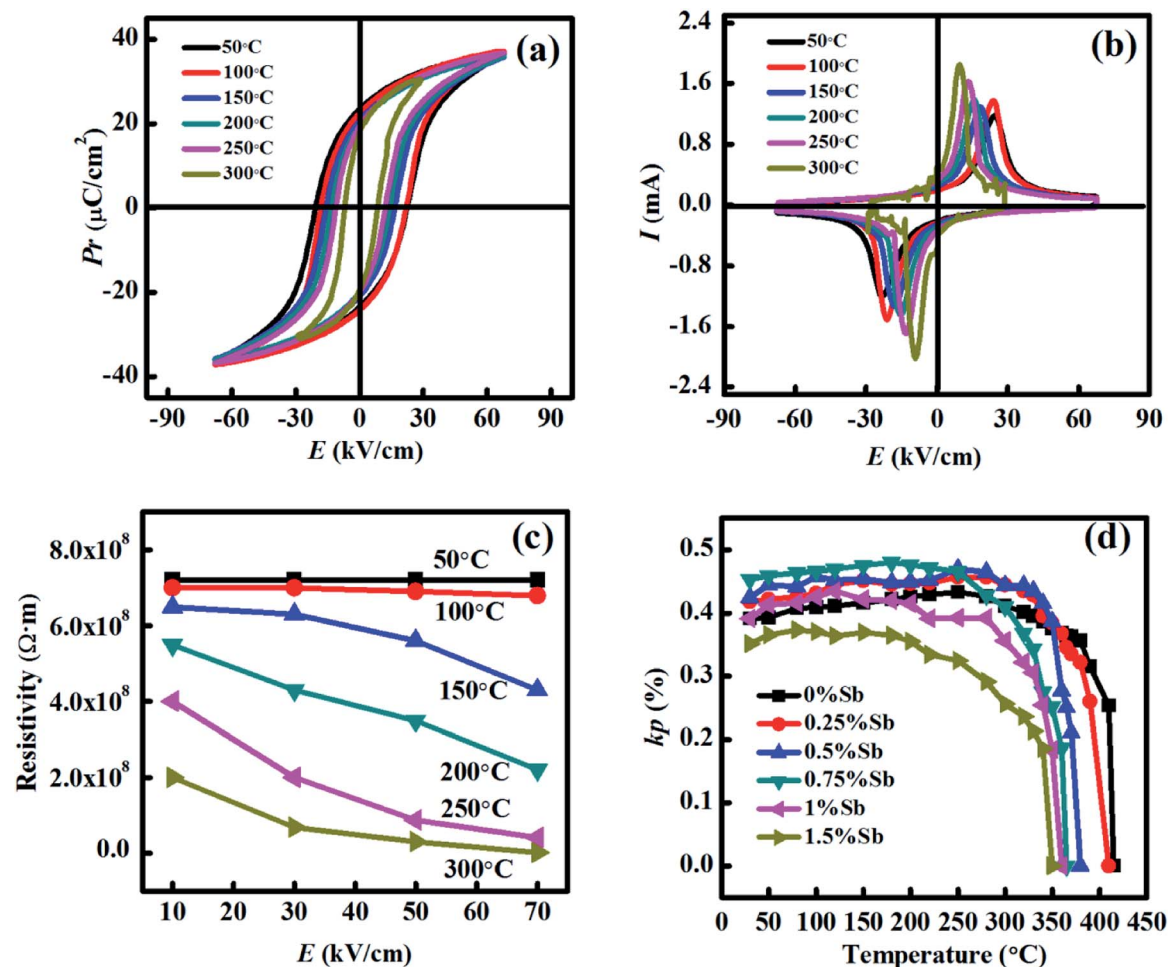
Fig. 6 (a) Temperature dependence of P–E hysteresis loops, (b) temperature dependence of I–E loops, (c) changes in resistivity, and (d) temperature dependence of k_p of BS–PTFMn + 0.75% Sb$_2$O$_3$ ceramics.

resulted from the reduction of the external effect, which was mainly due to the domain pinning caused by Fe/Mn doping.[21] While the increase in strain after Sb$_2$O$_3$ doping was attributed to releasing the domain wall pinning effect, which lead to an easier switch of the non-180° domain wall.[36] In addition, the large-signal piezoelectric coefficient d_{33}^* was calculated using the formula, $d_{33}^* = S_{max}/E_{max}$, from the S–E curves, as shown in Fig. 5(b). It was found that the variation of d_{33}^* with the Sb$_2$O$_3$ content was similar to that of the value of d_{33} measured by a quasi-static d_{33} meter. The maximum value of d_{33}^* was 442 pm

V^{-1} for BS–PTFMn + 0.75% Sb$_2$O$_3$ ceramics. The value of d_{33}^* was about 1.45-fold the d_{33} value (305 pC N^{-1}). The piezoelectric contributions of the ferroelectric materials contain two aspects: one is the intrinsic contribution due to the lattice distortion; the other is an extrinsic contribution due to the ferroelectric non-180° domain switching. The domain wall motion under a high electric field may provide a more extrinsic contribution to the overall piezoelectric properties. Accordingly, the large-signal d_{33}^* value is larger than that derived from the quasi-static piezo-electric meter.[39,40]

Table 3 Comparison of the electrical properties of BS–PTFMn + x% Sb$_2$O$_3$ and other BS–PT based ceramics

Sample	T_c (°C)	ε_r	tan δ	d_{33} (pC N^{-1})	k_p	T_d (°C)	Ref.
0.36BS–0.64 PT	450	2010	4%	460	0.56	250	14
0.36BS–0.64PTM	428	865	1%	254	0.47	230	17
Fe : 0.35BS–0.6PT–0.05PZN	440	1350	1.5%	220	0.33	—	41
0.10BT–0.36BS–0.54 PT	393	1890	8%	350	—	—	19
0.10PMN–0.30BS–0.60 PT	320	1000	4%	210	0.32	—	18
0.07PMS–0.33BS–0.60 PT	330	993	1.4%	225	0.38	—	20
BS–PTFMn + 0.75% Sb$_2$O$_3$	404	1230	1.4%	305	0.45	325	This work

3.4 Thermal stability

Thermal stability is interesting for sensors and actuators in various industrial applications. The temperature dependence of the P–E hysteresis loops of the BS–PTFMn + 0.75% Sb_2O_3 ceramics was measured with a frequency of 1 Hz, as shown in Fig. 6(a). BS–PTFMn + 0.75% Sb_2O_3 ceramics exhibited $P_r = 24$ $\mu C\ cm^{-2}$ and $E_c = 22\ kV\ cm^{-1}$ at room temperature. It was found that the P–E loops maintained a good square-shaped loop as the temperature increased, and there was no obvious leakage current caused by the reduction of the ceramic volume resistivity under high temperatures. At 300 °C, it is clearly seen that BS–PTFMn + 0.75% Sb_2O_3 ceramics maintained the values of P_r and E_c as high as 20 $\mu C\ cm^{-2}$ and 8.5 $kV\ cm^{-1}$, respectively. Fig. 6(b) shows the temperature dependence of the I–E loops of BS–PTFMn + 0.75% Sb_2O_3 ceramics. It is easily seen that standard I–E loops are shown below 300 °C. At 300 °C, the current curves fluctuated with several peaks under a high electric field, indicating that the leakage current starts to increase. Therefore, it is indicated that the ferroelectric properties of BS–PTFMn + 0.75% Sb_2O_3 ceramics start to degenerate at this temperature.

The high resistivity is necessary for high-temperature applications, particularly under a high electric field. The resistivity of BS–PTFMn + 0.75% Sb_2O_3 ceramics under a high electric field is shown in Fig. 6(c). It can be easily seen that the resistivity does not change at room temperature although the electric field was as high as 70 $kV\ cm^{-1}$, showing the resistivity of $7.2 \times 10^8\ \Omega\ m$, which satisfies the poling condition without any breakdown. The resistivity gradually decreased as the temperature increased. At 350 °C, though resistivity declined a lot under 70 $kV\ cm^{-1}$, the resistivity under 10 $kV\ cm^{-1}$ still maintained the value of $2.0 \times 10^8\ \Omega\ m$, showing a feature of an insulator. It is known that thermal stability is much affected by the large conductance in applications because it must work repeatedly under high temperatures. Therefore, the degradation of resistivity is responsible for the degradation of the piezoelectric performance of piezoelectric ceramics. It is concluded that the high resistivity of the BS–PTFMn + 0.75% Sb_2O_3 ceramics is in favor of the enhancement of the thermal stability of BS–PT ceramics.

To further characterize the temperature stability of the samples, the temperature dependence of k_p of the BS–PTFMn + x% Sb_2O_3 ceramics was measured (Fig. 6(d)). In this study, the value of the thermal depolarization temperature (T_d) of each sample was calculated, as listed in Table 2. Mostly, the fluctuation of the piezoelectric coefficient is required to be less than 10% for the industrial applications of piezoelectric ceramics. Therefore, T_d is defined as the temperature at which the value of kp dropped by 10%. It can be easily seen that the T_d value of BS–PTFMn + x% Sb_2O_3 ceramics decreased slightly as the Sb_2O_3 content increased, which was consistent with the change in the Curie temperature. However, T_d of all samples was still above 300 °C. For example, BS–PTFMn + 0.75% Sb_2O_3 ceramics exhibited T_d of 325 °C.

Table 3 shows the comparison of the electrical properties of BS–PTFMn + x% Sb_2O_3 and other BS–PT based ceramics. Compared with these systems with high d_{33} ($\geq$300 pC N^{-1}), BS–

PTFMn + 0.75% Sb_2O_3 ceramics exhibited a relatively low dielectric loss. In addition, BS–PTFMn + 0.75% Sb_2O_3 ceramics exhibited the highest d_{33} among these systems with a low dielectric loss ($\leq$1.5%). Therefore, the complex ion doping can improve the piezoelectric properties of BS–PT based ceramics. In addition, BS–PTFMn + 0.75% Sb_2O_3 ceramics exhibited a relatively high depolarization temperature. These results also confirm that the BS–PTFMn + x% Sb_2O_3 ceramics are promising piezoelectric materials for high-temperature applications.

4. Conclusions

The dielectric, ferroelectric, piezoelectric, and electromechanical coupling properties of the BS–PTFMn + x% Sb_2O_3 ceramics are presented in this study. The addition of Sb_2O_3 leads to BS–PTFMn + x% Sb_2O_3 ceramics transformed from the tetragonal phase to the rhombohedral phase. The relaxation enhancement was caused by the increase in Sb_2O_3, which was attributed to the increase in disorder in the perovskite structure. The BS–PTFMn + 0.75% Sb_2O_3 ceramics possessed optimal piezoelectric properties at room temperature, exhibiting $d_{33}^* = 442\ pm\ V^{-1}$. Although the Curie temperature of the system dropped slightly when Sb_2O_3 content increased, the thermal depolarization temperature (T_d) of BS–PTFMn + x% Sb_2O_3 ceramics remained above 300 °C, such as 325 °C for BS–PTFMn + x% Sb_2O_3 ceramics. These results also confirmed that doping with Sb_2O_3 can improve the piezoelectric properties of BS–PT piezoelectric ceramics. The results indicated that the dielectric constant, piezoelectric coefficient, electromechanical coupling factor increased and mechanical quality factor decreased after Sb_2O_3 doping. Therefore, the role of "soft" doping is the main effect of Sb_2O_3 on electrical performance. The enhanced piezoelectric properties and good thermal stabilities indicated that the BS–PTFMn + x% Sb_2O_3 ceramics are promising for high-temperature piezoelectric applications.

Conflicts of interest

There are no conflicts of interest to declare.

Acknowledgements

References

1 S. J. Zhang and F. P. Yu, Piezoelectric materials for high temperature sensors, *J. Am. Ceram. Soc.*, 2011, **94**, 3153–3170.

2 S. J. Zhang, X. N. Jiang, M. Lapsley, P. Moses and T. R. Shrout, Piezoelectric accelerometers for ultrahigh temperature application, *Appl. Phys. Lett.*, 2010, **96**, 013506.

3 D. Damjanovic, Materials for high temperature piezoelectric transducers, *Curr. Opin. Solid State Mater. Sci.*, 1998, **3**, 469–473.

4 J. F. Tressler, S. Alkoy and R. E. Newnham, Piezoelectric sensors and sensor materials, *J. Electroceram.*, 1998, **2**, 257–272.

5 R. C. Turner, P. A. Fuierer, R. E. Newnham and T. R. Shrout, Materials for high temperature acoustic and vibration sensors: a review, *Appl. Acoust.*, 1998, **41**, 299–324.

6 B. Noheda, D. E. Cox, G. Shirane, J. A. Gonzalo, L. E. Cross and S. E. Park, A monoclinic ferroelectric phase in the $Pb(Zr_{1-x}Ti_x)O_3$ solid solution, *Appl. Phys. Lett.*, 1999, **74**, 2059–2061.

7 R. E. Eitel, C. A. Randall, T. R. Shrout, P. W. Rehrig, W. Hackenberger and S. E. Park, New high temperature morphotropic phase boundary piezoelectrics based on $Bi(Me)O_3$–$PbTiO_3$ ceramics, *Jpn. J. Appl. Phys., Part 1*, 2001, **40**, 5999–6002.

8 M. R. Suchomel and P. K. Davies, Predicting the position of the morphotropic phase boundary in high temperature $PbTiO_3$-$Bi(B'B'')O_3$ based dielectric ceramics, *J. Appl. Phys.*, 2004, **96**, 4405–4410.

9 Z. Q. Hu, J. G. Chen, M. Y. Li, X. T. Li, G. X. Liu and S. X. Dong, Morphotropic phase boundary and high temperature dielectric, piezoelectric, and ferroelectric properties of $(1-x)Bi(Sc_{3/4}In_{1/4})O_3$-$xPbTiO_3$ ceramics, *J. Appl. Phys.*, 2011, **110**, 064102.

10 S. J. Zhang, R. Xia, C. A. Randall, T. R. Shrout, R. Duan and R. F. Speyer, Dielectric and piezoelectric properties of niobium-modified $BiInO_3$-$PbTiO_3$ perovskite ceramics with high Curie temperatures, *J. Mater. Res.*, 2005, **20**, 2067–2071.

11 F. Gao, R. Z. Hong and J. J. Liu, Phase formation and characterization of high Curie temperature $xBiYbO_3$–$(1-x)PbTiO_3$ piezoelectric ceramics, *J. Eur. Ceram. Soc.*, 2009, **29**, 1687–1693.

12 J. R. Cheng, W. Zhu, N. Li and L. E. Cross, Fabrication and characterization of $xBiGaO_3$-$(1-x)PbTiO_3$: a high temperature reduced Pb-content piezoelectric ceramic, *Mater. Lett.*, 2003, **57**, 2090–2094.

13 R. E. Eitel, S. J. Zhang, T. R. Shrout, C. A. Randall and I. Levin, Phase diagram of the perovskite system $(1-x)BiScO_3$-$xPbTiO_3$, *J. Appl. Phys.*, 2004, **96**, 2828–2831.

14 R. E. Eitel, C. A. Randall, T. R. Shrout and S. E. Park, Preparation and characterization of high temperature perovskite ferroelectrics in the solid-solution $(1-x)BiScO_3$-$xPbTiO_3$, *Jpn. J. Appl. Phys., Part 1*, 2002, **41**, 2099–2104.

15 B. Kowalski and A. Sehirlioglu, High temperature limitation due to onset of depoling in $BiScO_3$-$PbTiO_3$, *J. Appl. Phys.*, 2017, **121**, 064106.

16 S. W. Gotmare, S. O. Leontsev and R. E. Eitel, Thermal degradation and aging of high-temperature piezoelectric ceramics, *J. Am. Ceram. Soc.*, 2010, **93**, 1965–1969.

17 J. G. Chen, Z. Q. Hu, H. D. Shi, M. Y. Li and S. X. Dong, High-power piezoelectric characteristics of manganese-modified $BiScO_3$-$PbTiO_3$ high-temperature piezoelectric ceramics, *J. Phys. D: Appl. Phys.*, 2012, **45**, 465303.

18 J. Ryu, S. Priya, C. Sakaki and K. Uchino, High power piezoelectric characteristics of $BiScO_3$-$PbTiO_3$-$Pb(Mn_{1/3}Nb_{2/3})O_3$, *Jpn. J. Appl. Phys., Part 1*, 2002, **41**, 6040–6044.

19 H. Qiao, C. He, Z. Wang, X. Li, Y. Liu and X. Long, Improved electrical properties of $BaTiO_3$ modified $BiScO_3$-$PbTiO_3$ ceramics with high Curie temperature, *Ceram. Int.*, 2017, **43**, 11463–11468.

20 B. L. Deng, Q. Wei, C. He, Z. J. Wang, X. M. Yang and X. F. Long, Effect of $Pb(Mn_{1/3}Sb_{2/3})O_3$ addition on the electrical properties of $BiScO_3$-$PbTiO_3$ piezoelectric ceramics, *J. Alloys Compd.*, 2019, **790**, 397–404.

21 G. Chen, G. X. Jin, C. M. Wang and J. R. Cheng, Reduced dielectric loss and strain hysteresis in Fe and Mn commodified high-temperature $BiScO_3$-$PbTiO_3$ ceramics, *J. Am. Ceram. Soc.*, 2014, **97**, 3890–3896.

22 M. M. Nadoliisky, T. K. Vassileva and P. B. Vitkov, Dielectric, piezoelectric and pyroelectric properties of $PbZrO_3$-$PbTiO_3$-$Pb(Mn_{1/3}Sb_{2/3})O_3$ ferroelectric system, *Ferroelectrics*, 1992, **129**, 141–146.

23 Z. G. Zhu, N. Z. Zheng, G. R. Li and Q. R. Yin, Dielectric and electrical conductivity properties of PMS-PZT ceramics, *J. Am. Ceram. Soc.*, 2006, **89**, 717–719.

24 Y. K. Gao, Y. H. Chen, J. Ryu, K. Uchino and D. Viehland, Eu and Yb substituent effects on the properties of $Pb(Zr_{0.52}Ti_{0.48})O_3$-$Pb(Mn_{1/3}Sb_{2/3})O_3$ ceramics: development of a new high-power piezoelectric with enhanced vibrational velocity, *Jpn. J. Appl. Phys., Part 1*, 2001, **40**, 687–693.

25 W. M. Zhu and Z. G. Ye, Improved dielectric and ferroelectric properties of high curie temperature $(1-x)BiFeO_3$-$xPbTiO_3$ Ceramics by aliovalent ionic substitution, *Appl. Phys. Lett.*, 2006, **89**, 232904.

26 H. Abid, S. Nidhi, J. J. Abhilash, D. Komal, G. Sahil and K. Binay, Improvement in dielectric, piezoelectric and ferroelectric properties of 0.64PMN–0.36PT ceramics by Sb modification, *J. Mater. Sci.*, 2017, **28**, 14298–14307.

27 Z. Ren and Z. G. Ye, Effects of Mn-Doping on PIN-PMN-PT ceramics with MPB composition, *Ferroelectrics*, 2014, **464**, 130–135.

28 G. Arlt, D. Hennings and G. Dewith, Dielectric properties of fine-grained barium titanate ceramics, *J. Appl. Phys.*, 1985, **58**, 1619–1625.

29 T. Hoshina, K. Takizawa and J. Li, Domain size effect on dielectric properties of barium titanate ceramics, *Jpn. J. Appl. Phys.*, 2008, **47**, 7607.

30 Y. A. Huang, B. Lu and Y. X. Zou, Grain size effect on dielectric, piezoelectric and ferroelectric property of $BaTiO_3$ ceramics with fine grains, *J. Inorg. Mater.*, 2018, **33**(7), 767.

31 G. Viola, K. B. Chong, M. Eriksson, Z. J. Shen, J. T. Zeng and Q. R. Yin, Effect of grain size on domain structures, dielectric and thermal depoling of Nd-substituted bismuth titanate ceramics, *Appl. Phys. Lett.*, 2013, **103**, 182903.

32 Z. Ai, Y. Hou, M. Zheng and M. Zhu, Effect of grain size on the phase structure and electrical properties of PZT-PNZN quaternary systems, *J. Alloys Compd.*, 2014, **617**, 222.

33 X. G. Tang, K. H. Chew and H. L. W. Chan, Diffuse phase transition and dielectric tunability of Ba(Zr$_y$Ti$_{1-y}$)O$_3$ relaxor ferroelectric ceramics, *Acta Mater.*, 2004, **52**, 5177–5183.

34 T. Shi, L. Xie, L. Gu and J. Zhu, Why Sn doping significantly enhances the dielectric properties of Ba(Ti$_{1-x}$Sn$_x$)O$_3$, *Sci. Rep.*, 2014, **5**, 8606.

35 Y. H. Jiang, Y. Zhao, B. Q. Qin, Y. Z. Jiang, W. Shi, L. H. Li, D. Q. Xiao and J. G. Zhu, Dielectric and piezoelectric properties of (1-x)(Bi$_{1-y}$Li$_y$)(Sc$_{1-y}$Sb$_y$)O$_3$-xPbTiO$_3$ high-temperature relaxor ferroelectric ceramics, *Appl. Phys. Lett.*, 2008, **93**, 022904.

36 Q. M. Zhang, H. Wang, N. Kim and L. E. Cross, Direct evaluation of domain-wall and intrinsic contributions to the dielectric and piezoelectric response and their temperature-dependence on lead-zirconate-titanate ceramics, *J. Appl. Phys.*, 1994, **75**, 454.

37 G. H. Haertling, Ferroelectric ceramics: History and Technology, *J. Am. Ceram. Soc.*, 1999, **82**, 797–818.

38 S.-E. Park and T. R. Shrout, Characteristics of relaxor-based piezoelectric single crystals for ultrasonic transducers, *IEEE Trans. Ultrason. Ferroelectr. Freq. Control*, 1997, **44**, 1140–1147.

39 J. G. Chen, T. L. Zhao, J. R. Cheng and S. X. Dong, Enhanced piezoelectric performance of (0.98-x)Bi(Sc$_{3/4}$In$_{1/4}$)O$_3$-xPbTiO$_3$-0.02Pb(Zn$_{1/3}$Nb$_{2/3}$)O$_3$ ternary high temperature piezoelectric ceramics, *J. Appl. Phys.*, 2013, **113**, 5.

40 A. Jalalian, A. M. Grishin, X. L. Wang, Z. X. Cheng and S. X. Dong, Large piezoelectric coefficient and ferroelectric nanodomain switching in Ba(Ti$_{0.80}$Zr$_{0.20}$)O$_3$-0.5(Ba$_{0.70}$Ca$_{0.30}$)TiO$_3$ nanofibers and thin films, *Appl. Phys. Lett.*, 2014, **104**, 103112.

41 Q. W. Liao, X. S. Chen, X. C. Chu, F. Zeng and D. Guo, Effect of Fe Doping on the Structure and Electric Properties of Relaxor Type BSPT-PZN Piezoelectric Ceramics Near the Morphotropic Phase Boundary, *Sens. Actuators, A*, 2013, **201**, 222–229.